Inorganic Chemistry

Article

pubs.acs.org/IC

Metal Insertion in a Methylamine-Functionalized Zirconium Metal–Organic Framework for Enhanced Carbon Dioxide Capture

A. Paulina Gómora-Figueroa,*[,†,‡] Jarad A. Mason,[†] Miguel I. Gonzalez,[†] Eric D. Bloch,[†] and Katie R. Meihaus[†]

[†]Department of Chemistry, University of California, Berkeley, Berkeley, California 94720, United States

[‡]División de Ingeniería en Ciencias de la Tierra, Facultad de Ingeniería, Universidad Nacional Autónoma de México, Circuito Exterior, Ciudad Universitaria, 04510, Ciudad de México, México

Supporting Information

ABSTRACT: The reaction of $ZrCl_4$ with 2′,3′,5′,6′-tetramethylamino-*p*-terphenyl-4,4″-dicarboxylic acid (H_2tpdc-$4CH_2NH_2{\cdot}3HCl$) in the presence of NaF affords $Zr_6O_4(OH)_{2.1}F_{1.9}$(tpdc-$4CH_2NH_2{\cdot}3HCl)_6$ (**1**), which is a new member of the $Zr_6O_4(OH)_4$(dicarboxylate linker)$_{12}$ or UiO-68 family, and exhibits high porosity with BET and Langmuir surface areas of 1910 m^2/g and 2220 m^2/g, respectively. Remarkably, fluoride ion incorporation in the zirconium clusters results in increased thermal stability, marking the first example of enhancement in the stability of a UiO framework by this defect-restoration approach. Although material **1** features four alkylamine groups on each organic linker, the framework does not exhibit the high CO_2 uptake that would be expected for reaction between CO_2 and the amine groups to form carbamic acid or ammonium carbamate species. The absence of strong CO_2 adsorption can likely be attributed to protonation at some of the amine sites and the presence of counterions. Indeed, exposure of material **1** to acetonitrile solutions of the organic bases 1,8-bis(dimethylamino)naphthalene (DMAN) or trimethylamine, affords a partially deprotonated material, which exhibits enhanced CO_2 uptake. Exposure of basic amine sites also facilitates the postsynthetic chelation of copper(I) ($[Cu(MeCN)_4]{\cdot}CF_3SO_3$) to yield material **2** with an enhanced CO_2 uptake of 4 wt % at 0.15 bar, which is double that of the parent framework **1**.

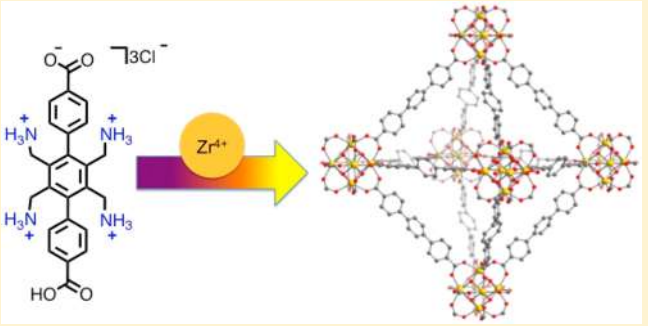

INTRODUCTION

As anthropogenic carbon dioxide (CO_2) emissions continue to rise, significant effort is being directed toward the development of materials that can selectively and efficiently adsorb CO_2 under conditions relevant to carbon capture from power plants.[1] Indeed, existing coal- and gas-fired power plants are responsible for 60% of annual global CO_2 emissions,[1a] and thus carbon capture (and subsequent storage) from these stationary sources could contribute substantially to a reduction in emissions and detrimental global climate change. Currently, the most developed and readily implemented technology is for postcombustion CO_2 capture, where the principal flue gas components, by volume, are N_2 (73–77%), CO_2 (~15%), H_2O (5–7%), O_2 (3–4%), and SO_2/NO_x (<0.08%), with total pressures near 1 bar and temperatures between 40 and 60 °C.[2]

At present, aqueous amine solutions are employed in the separation of CO_2 from postcombustion gas mixtures, and these solutions exhibit extremely high selectivity for CO_2. However, significant energy is required to regenerate these aqueous solutions due primarily to their large heat capacities.[3] Solid adsorbents present a promising alternative and have been extensively evaluated for postcombustion CO_2 capture due to their significantly smaller heat capacities, which may substantially reduce material regeneration energies.[4,2b] In particular, the introduction of alkylamine functional groups onto adsorbent surfaces can lead to materials with high selectivity for CO_2 over N_2. These functional groups are particularly promising as they are expected to exhibit high affinity and selectivity for CO_2 even in the presence of H_2O.[5]

Among the different classes of solid adsorbents, metal–organic frameworks have recently received significant attention for CO_2 separations, owing to their unique structural diversity, high surface areas, and chemical tunability. Frameworks that feature coordinatively unsaturated metal centers on the pore surface are especially promising, due to the exceptional gas uptake afforded by these Lewis acidic metal sites.[6] Moreover, these sites are also amenable to postsynthetic functionalization to further enhance their ability to selectively capture CO_2.[7] Indeed, it has been reported that *N*,*N*′-dimethylethylenediamine (mmen) functionalization at the open metal sites of the framework M_2(dobpdc) (dobpdc^{4-} = 4,4′-dioxidobiphenyl-3,3′-dicarboxylate, M = Mg, Mn, Fe, Co, Zn) yields a series of "phase-change" adsorbents, which exhibit step-shaped iso-

Received: November 13, 2016
Published: March 27, 2017

DOI: 10.1021/acs.inorgchem.6b02745
Inorg. Chem. 2017, 56, 4308–4316

therms arising from cooperative formation of ammonium carbamate chains along the channels of the framework upon selective CO_2 adsorption.[8]

In addition, the previously reported Al(OH) (bpydc) (bpydc^{2-} = 4,4′-bipyridinedicarboxylate) material, which features open bipyridine sites on the organic linkers can postsynthetically coordinate metal cations. Notably, metalation of the framework with $Cu(BF_4)_2$ resulted in increased CO_2 capacity and selectivity for CO_2 over N_2.[9] Inspired by these results, and the fact that the direct formation of metal−organic frameworks bearing open chelation sites is rare, we sought to synthesize a metal−organic framework exhibiting a high density of methylamines as potential strong CO_2 binding sites that could also be used to postsynthetically bind metal cations.

Herein, we report the synthesis of the ligand 2′,3′,5′,6′-tetramethylamino-*p*-terphenyl-4,4″-dicarboxylic acid (Scheme S1) and its successful incorporation as a linker in the robust zirconium metal−organic framework, **1**, which adopts the structural motif of UiO-68, $[Zr_6(O)_4(OH)_4(ligand)_6]$[10] and represents the first example of a metal−organic framework with a high density of covalently attached alkylamine functionalities.[11] Material **1** exhibits moderate uptake of CO_2 at low pressures and postsynthetic metalation of this material with $Cu(MeCN)_4{\cdot}CF_3SO_3$ results in enhanced CO_2 adsorption properties that are discussed in detail. In addition, fluoride ions were successfully incorporated into the inorganic zirconium cluster as bridging anions and found to impart enhanced thermal stability over the hydroxide-bridged clusters.

EXPERIMENTAL DETAILS

All reagents were obtained from commercial vendors and used without further purification unless otherwise noted. *N*-Bromosuccinimide was recrystallized prior to use. Ultrahigh purity grade (99.998% purity or higher) carbon dioxide, nitrogen, and helium were used for the adsorption measurements. Gas adsorption data were obtained by volumetric methods using a Micromeritics ASAP-2020 instrument. Isotherms at 77 K were measured in liquid nitrogen baths. Isotherms at 25, 35, and 45 °C were measured using a water circulator to maintain a constant temperature. Thermogravimetric analyses (TGAs) were carried out under a nitrogen flow with a TA Instruments TGA Q5000 (carbon dioxide 98% purity was used for cyclability experiments). Powder X-ray diffraction patterns were collected on a Bruker D8 Advance diffractometer with a Cu anode (1.5406 Å). Infrared spectra were obtained on a PerkinElmer Spectrum 100 Optica FTIR spectrometer furnished with attenuated total reflectance (ATR).

Synthesis of 2′,3′,5′,6′-tetramethyl-*p*-terphenyl-4,4″-dicarboxylic Ester (tpdc-4CH$_2$CH$_3$). 1,4-Diiodo-2′,3′,5′,6′-tetramethylbenzene (10.0 g, 25.9 mmol) and cesium fluoride (31.5 g, 20.7 mmol) were placed in a Schlenk flask, which was evacuated for 2 h and then purged with N_2 for 30 min. The solids were then dissolved in a p-dioxane/H_2O mixture (150 mL/75 mL), and a suspension of [1,1′-bis(diphenylphosphino)ferrocene]palladium(II) dichloride (1.06 g, 1.30 mmol) and 4-methoxycarbonylphenylboronic acid (9.32 g, 51.8 mmol) in a p-dioxane/H_2O mixture (2:1, 200 mL) was added to the solution. The resulting mixture was heated to reflux for 8 h under a N_2 atmosphere. After cooling to room temperature, the reaction mixture was filtered, and the product was washed with brine and then water. The resulting powder was dissolved in chloroform, and the remaining black precipitate was filtered. Finally, the solvent was removed, and the resulting precipitate was rinsed several times with acetone and then hexanes to give tpdc-4CH$_2$CH$_3$ as a white microcrystalline powder (9.1 g, 91%). Melting point (Mp): >240 °C. Elemental analysis calculated for $C_{26}H_{26}O_4$ (402.48 g/mol): C, 77.59; H, 6.51. Found: C, 77.53; H, 6.73. ^{1}H NMR (400 MHz, $CDCl_3$, TMS, room temperature (rt)): δ 8.14 (d, J = 8.0 Hz, 4H, Ar*H*), 7.28 (d, J = 8.0 Hz, 4H, Ar*H*), 3.97 (s, 6H, O*CH*$_3$), 1.93 (s, 12H Ar*CH*$_3$).

Synthesis of 2′,3′,5′,6′-Tetramethylboro-*p*-terphenyl-4,4″-dicarboxylic Ester (tpdc-4CH$_2$Br). tpdc-4CH$_2$CH$_3$ (6.00 g, 14.9 mmol) and *N*-bromosuccinimide (11.6 g, 65.2 mmol) were added to a Schlenk flask, which was evacuated for 1.5 h. The system was purged with nitrogen, and the mixture was suspended in anhydrous benzene (150 mL). After stirring the mixture for 30 min, azobis-(isobutyronitrile) was added (5 mol %), and the suspension was heated to reflux for 20 h under a N_2 atmosphere. After cooling the reaction mixture to room temperature, the resulting product was filtered and washed with cold methanol to give compound tpdc-4CH$_2$Br as a white powder (9.4 g, 87%). Mp: >240 °C. Elemental analysis calculated for $C_{26}H_{22}Br_4O_4$ (718.07 g/mol): C, 43.49; H, 3.09. Found: C, 44.61; H, 3.48. ^{1}H NMR (400 MHz, $CDCl_3$, TMS, rt): δ 8.22 (d, J = 8.0 Hz, 4H, Ar*H*), 7.55 (d, J = 8.0 Hz, 4H, Ar*H*), 4.33 (s, 8H Ar*CH*$_2$Br), 3.99 (s, 6H, O*CH*$_3$).

Synthesis of 2′,3′,5′,6′-Tetramethylazido-*p*-terphenyl-4,4″-dicarboxylic Ester (tpdc-4CH$_2$N$_3$). A mixture of tpdc-4CH$_2$Br (6.0 g, 8.3 mmol) and sodium azide (2.4 g, 37 mmol) was suspended in anhydrous DMF (600 mL) and stirred at 60 °C for 6 h under N_2 atmosphere. After the solution was cooled to room temperature, the solvent was removed by filtration, and the product was rinsed with brine and water to obtain compound tpdc-4CH$_2$N$_3$ as white needles (4.0 g, 85%). Mp: 190 °C (decomposition). Elemental analysis calculated for $C_{26}H_{22}N_{12}O_4$ (566.53 g/mol): C, 55.12; H, 3.91; N, 29.67. Found: C, 55.37; H, 4.19; N, 28.96. ^{1}H NMR (400 MHz, $CDCl_3$, TMS, rt): δ 8.23 (d, J = 8.0 Hz, 4H, Ar*H*), 7.40 (d, J = 8.0 Hz, 4H, Ar*H*), 4.23 (s, 8H Ar*CH*$_2$N), 3.99 (s, 6H, O*CH*$_3$). IR (solid-ATR, cm^{-1}): 2102 (ν_{as} N$_3$), 1717 (ν C═O), 1256 (ν_s N$_3$), 1100 (ν_s C−O−R), 1121 (ν_{as} C−O−R).

Synthesis of 2′,3′,5′,6′-Tetramethylazido-*p*-terphenyl-4,4″dicarboxylic Acid (H$_2$tpdc-4CH$_2$N$_3$). tpdc-4CH$_2$N$_3$ (4.0 g, 7.1 mmol) and KOH (1.6 g, 28 mmol) were suspended in a 2:1 THF/water mixture. The reaction mixture was stirred for 72 h at room temperature. Subsequently, 3 M HCl was added slowly until a pH of 1 was reached. The THF was then removed under vacuum, and the remaining reaction mixture was filtered. The resulting white powder (H$_2$tpdc-4CH$_2$N$_3$) was rinsed several times with distilled water and dried overnight in air (3.4 g, 90%). Mp: 215 °C (decomposition). Elemental analysis calculated for $C_{24}H_{20}N_{12}O_4{\cdot}(0.5THF)(H_2O)$ (592.55 g/mol): C, 52.70; H, 4.08; N, 28.37. Found: C, 52.64; H, 3.90; N, 28.00. ^{1}H NMR (400 MHz, DMSO, TMS, rt): δ 13.18 (s, 2H, COO*H*), 8.12 (d, J = 8.0 Hz, 4H, Ar*H*), 7.41 (d, J = 8.0 Hz, 4H, Ar*H*), 4.30 (s, 8H Ar*CH*$_2$N). IR (solid-ATR, cm^{-1}): 2960 (ν O−H), 2093 (ν_{as} N$_3$), 1676 (ν C═O), 1425 (δ O−H), 1267 (ν_s N$_3$).

Synthesis of 2′,3′,5′,6′-Tetramethylammonium-*p*-terphenyl-4,4″-dicarboxylate (H$_2$tpdc-4CH$_2$NH$_2$). Triphenylphosphine (4.3 g, 16 mmol) and H$_2$tpdc-4CH$_2$N$_3$ (2.0 g, 3.7 mmol) were dissolved in a mixture of freshly distilled THF (200 mL) and water (150 mL) and stirred for 72 h at room temperature. The resulting suspension was then filtered and washed with isopropanol to obtain H$_2$tpdc-4CH$_2$NH$_2$ as a white powder (1.2 g, 70%). Mp: >300 °C. Elemental analysis calculated for $C_{24}H_{26}N_4O_4{\cdot}(5H_2O)(^iPrOH)$ (566.64 g/mol): C, 57.23; H, 7.47; N, 9.89. Found: C, 57.50; H, 6.90; N, 9.76. IR (solid-ATR, cm^{-1}): 3344 (ν_{as} NH$_2$), 3262 (ν_s NH$_2$), 2917 (ν NH$_3^+$), 1583 (ν C═O), 1534 (δ NH$_2$).

Synthesis of 2′,3′,5′,6′-Tetramethylamino-*p*-terphenyl-4,4″-dicarboxylic Acid (H$_2$tpdc-4CH$_2$NH$_2$·3HCl). Compound H$_2$tpdc-4CH$_2$NH$_2$ (1.2 g, 2.8 mmol) was suspended in distilled water (25 mL) to which 3 M HCl was added until a pH of 1 was reached. The resulting solution was stirred for 30 min after which all volatiles were removed under vacuum to give H$_2$tpdc-4CH$_2$NH$_2$·3HCl as a pale green microcrystalline powder (1.3 g, 83%). Mp: >240 °C (decomposition). Elemental analysis calculated for $C_{24}H_{29}Cl_3N_4O_4$ (543.87 g/mol): C, 53.00; H, 5.37; N, 10.30; Cl, 19.56. Found: C, 52.36; H, 5.13; N, 9.63; Cl, 20.00. ^{1}H NMR (400 MHz, DMSO, TMS, rt): δ 13.25 (s, 2H, COO*H*), 8.45 (s, 11H, N*H*$_x$), 8.12 (d, J = 8.0 Hz, 4H, Ar*H*), 7.66 (d, J = 8.0 Hz, 4H, Ar*H*), 3.96 (s, 8H Ar*CH*$_2$N). IR (solid-ATR, cm^{-1}): 3364 (ν_{as} NH$_2$), 2868, 2611 (ν NH$_3^+$), 1696 (ν C═O), 1608 (δ NH$_2$), 1226 (ν_s C$_{alkyl}$−N). Mass spectrometry (MS): 435.20 m/z (M$^+$), 218.10 m/z (M^{2+}), 145.05 m/z (M^{3+}).

DOI: 10.1021/acs.inorgchem.6b02745
Inorg. Chem. 2017, 56, 4308−4316

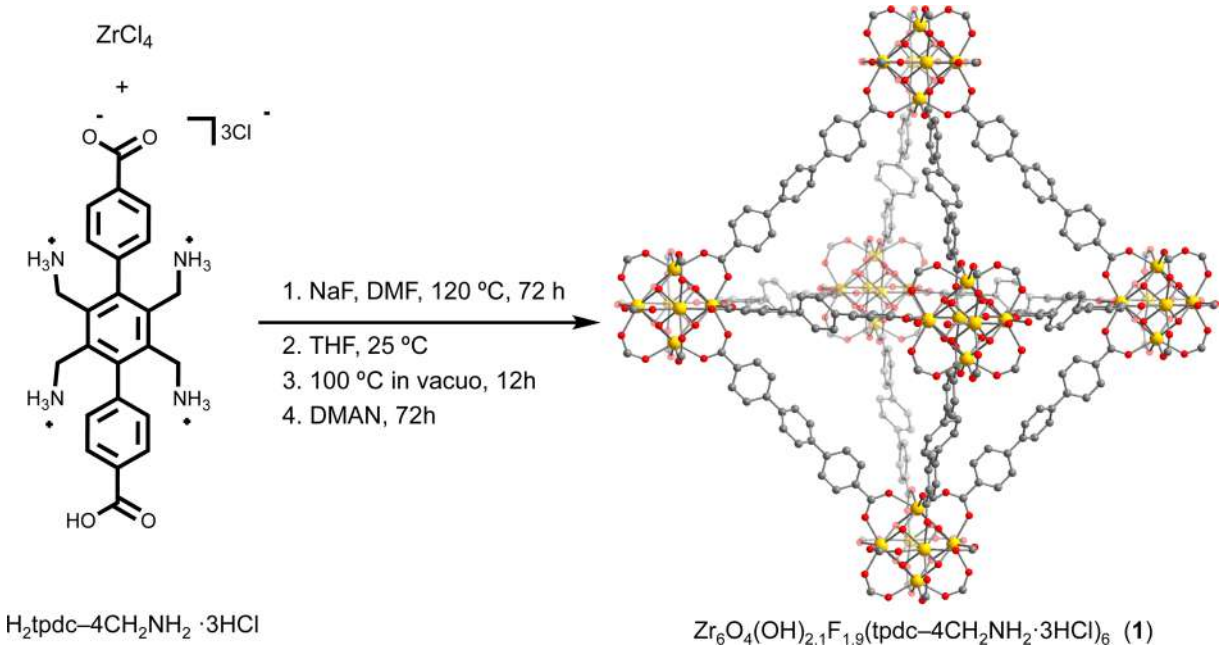

Figure 1. (Left) Synthesis conditions for $Zr_6O_4(OH)_{2.1}F_{1.9}(tpdc\text{-}4CH_2NH_2{\cdot}2HCl)_6$ (**1**), ($tpdc^{4-}$ = 2′,3′,5′,6′-tetramethylamino-*p*-terphenyl-4,4″-dicarboxylate), using the zwitterionic form of the ligand. (Right) Proposed structure of **1**, where the framework structural model is obtained from the crystal structure of UiO-68.[10a] The methyl amino groups of $H_2tpdc\text{-}4CH_2NH_2{\cdot}3HCl$ are not depicted.

Synthesis of $Zr_6O_4(OH)_{2.1}F_{1.9}(tpdc\text{-}4CH_2NH_2{\cdot}2HCl)_6$ (1). $Zr_6O_4(OH)_{2.1}F_{1.9}(tpdc\text{-}4CH_2NH_2{\cdot}2HCl)_6$ (**1**), can be synthesized from either $H_2tpdc\text{-}4CH_2NH_2$ or $H_2tpdc\text{-}4CH_2NH_2{\cdot}3HCl$. The procedure herein describes the synthesis using 2′,3′,5′,6′-tetramethylammonium-*p*-terphenyl-4,4″-dicarboxylate ($H_2tpdc\text{-}4CH_2NH_2$) as ligand. Benzoic acid is included to achieve optimal crystallinity.[10b] A solution of $ZrCl_4$ (96 mg, 0.41 mmol) and benzoic acid (1.85 g, 15.2 mmol) in 15 mL of *N*,*N*′-dimethylformamide (DMF) was added to a 20 mL scintillation vial containing 2′,3′,5′,6′-tetramethylammonium-*p*-terphenyl-4,4″-dicarboxylate (120 mg, 0.28 mmol) and sodium fluoride (7.0 mg, 0.17 mmol). The reaction mixture was sonicated for 20 min and then heated on a hot plate at 120 °C for 72 h. The resulting white microcrystalline powder was then filtered and washed five times with DMF and then THF.

Lastly, **1** was stirred with a 1,8-bis(dimethylamino)naphthalene (DMAN) or triethylamine solution in acetonitrile (0.21 M) for 72 h. Then the supernatant was decanted and solvent exchanges were carried out with fresh acetonitrile followed by THF. Each solvent was exchanged three times, every 24 h, after which the material was collected by filtration under inert atmosphere and heated at 100 °C for 12 h under vacuum. Yield: 160 mg (70%). Elemental analysis calculated for $(C_{24}H_{27}N_4O_4Cl_2)_6(O)_4F_{1.9}(OH)_{2.1}Zr_6{\cdot}7(C_7H_5O_2)$ (4569.36 g/mol): C, 50.73; H, 4.39; N, 7.36. Found: C, 51.03; H, 4.01; N, 7.49. IR (solid-ATR, cm^{-1}): 3135 (ν_{as} NH_2), 2906, 2826, 2753 (ν NH_3^+), 1686 (ν C═O), 1609 (δ NH_2), 1418 (δ_{as} NH_3^+), 523 (ν Zr−F).

Synthesis of $Zr_6O_4(OH)_{2.1}F_{1.9}(tpdc\text{-}4CH_2NH_2{\cdot}1.9HCl)_6{\cdot}0.42Cu(MeCN)_4{\cdot}CF_3SO_3$ (2). Material **1** (0.20 g, 0.26 mmol) and $Cu(MeCN)_4{\cdot}CF_3SO_3$ (18 mg, 0.026 mmol), were suspended together in tetrahydrofuran (15 mL) and heated on a hot plate at 80 °C for 7 days. The resulting yellow solid was collected by filtration and soaked in 15 mL of fresh THF. The solvent was exchanged every 24 h for a total of 3 days, and then the colorless supernatant was decanted and the solid was heated at 140 °C for 12 h under vacuum. Yield: 180 mg (89%). Elemental analysis calculated for $(C_{24}H_{27}N_4O_4Cl_{1.9})_6F_{1.9}(OH)_{2.1}(O)_4Zr_6{\cdot}7(C_7H_5O_2){\cdot}0.42Cu(MeCN)_4{\cdot}CF_3SO_3$ (4706.35 g/mol): C, 50.22; H, 4.37; N, 7.64; Cu, 0.57. Found: C, 51.03; H, 4.01; N, 7.49; Cu, 0.58. IR (solid-ATR, cm^{-1}): 3135 (ν_{as} NH_2), 2906, 2826, 2753(ν NH_3^+), 1686 (ν C═O), 1609 (δ NH_2), 1415 (δ_{as} NH_3^+), 1280 (ν C−F), 1052 (ν S═O), 536 (ν Zr−F), 483 (ν Cu−O).

Synthesis of $Zr_6O_4(OH)_{2.1}F_{1.9}(tpdc\text{-}4CH_2NH_2{\cdot}1.7HCl)_6{\cdot}1.8Cu(CF_3SO_3)_2$ (3). Tetrahydrofuran (15 mL) was added to a 20 mL scintillation vial containing a solid mixture of **1** (0.10 g, 0.13 mmol) and $Cu(CF_3SO_3)_2$ (14 mg, 0.034 mmol). The mixture was heated on a hot plate at 80 °C for 7 days. The resulting blue solid was collected by filtration and soaked in 15 mL of tetrahydrofuran. After 24 h, the supernatant was decanted and replaced with fresh tetrahydrofuran. The solvent was exchanged two times, such that the total soaking time was 3 days, after which the product was collected and heated at 140 °C for 12 h under vacuum. Yield: 80 mg (72%). Elemental analysis calculated for $(C_{24}H_{27}N_4O_4Cl_{1.7})_6F_{1.9}(OH)_{2.1}(O)_4Zr_6{\cdot}7(C_7H_5O_2){\cdot}1.8Cu(CF_3SO_3)_2$ (5156.57 g/mol): C, 45.79; H, 3.89; N, 6.52; Cu, 2.22. Found: C, 45.13; H, 3.49; N, 6.93; Cu, 2.18. IR (solid-ATR, cm^{-1}): 2973, 2876 (ν NH_3^+), 1688 (ν C═O), 1611 (δ NH_2), 1420 (δ_{as} NH_3^+), 1266 (ν C−F), 1018 (ν S═O), 531 (ν Zr−F), 470 (ν Cu−O).

RESULTS AND DISCUSSION

Synthesis and Structural Characterization. The synthesis of $Zr_6O_4(OH)_{2.1}F_{1.9}(tpdc\text{-}4CH_2NH_2{\cdot}3HCl)_6$ (**1**), was accomplished by reacting $ZrCl_4$ with benzoic acid and either the zwitterionic ($H_2tpdc\text{-}4CH_2NH_2$) or the neutral form ($H_2tpdc\text{-}4CH_2NH_2{\cdot}3HCl$) of the ligand at 120 °C for 72 h in DMF (Figure 1). Benzoic acid was added, which has been shown to improve the crystallinity of UiO materials. The formation of a metal−organic framework isostructural to UiO-68 was confirmed by powder X-ray diffraction (Figure S11). Although it has been previously reported that benzoic acid promotes the formation of destabilizing defects within the inorganic cluster of the UiO-66 structure type,[12,10b] in our hands the absence of benzoic acid led only to amorphous materials, while the use of other acid sources resulted in materials with either poor crystallinity or diminished porosity.[13] Notably, the material **1** exhibits a more pronounced sensitivity toward air and water and a lower thermal stability than expected when compared with its structural analogue, UiO-66. We hypothesized that the lack of stability is due to the formation of defects in the inorganic cluster under our

DOI: 10.1021/acs.inorgchem.6b02745
Inorg. Chem. 2017, 56, 4308−4316

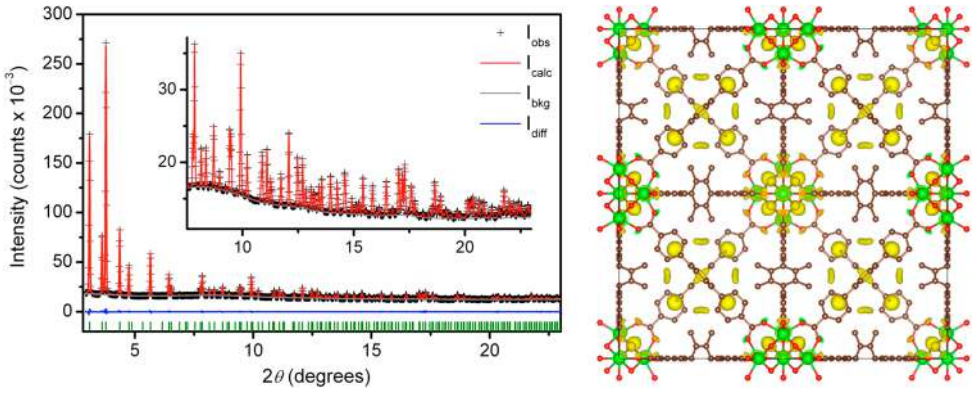

Figure 2. (Left) Structureless Le Bail refinement of the X-ray powder diffraction pattern of desolvated **1**, which results in a unit cell similar to UiO-68 (*Fm*-3m, 32.4668(3) Å, V = 34223(1) Å^3). The calculated powder pattern (red line) is in good agreement with the experimental data (pluses) as evidenced by the difference pattern (blue line) and calculated peak positions (green tick marks). (Right) Electron Fourier difference map for **1** using PCN-57 as a structural model.[17] Unidentified electron density is shown in yellow and is attributed to $-NH_2$, $-NH_3^+$, and Cl^- inside the framework pores. Green, brown, and red spheres represent Zr, C, and O atoms, respectively; H atoms have been omitted for clarity.

particular synthesis conditions. In addition, it has been reported that the chemical and thermal stability of the zirconium MOFs can be significantly altered by the functional groups attached to as well as the length of the organic linker.[12b,d] In some cases, the resulting MOFs become more susceptible to chemical degradation by water, polar solvents, NaOH and HCl.[12c] For instance, UiO-66-NH_2 has a considerably lower thermal stability than UiO-66, likely due to the weakening of the C−C bonds between the aromatic ring and the carboxylate group due to the inductive effect of the $-NH_2$ group.[12c]

Therefore, in an effort to improve the stability of the resulting metal−organic framework, **1**, we added sodium fluoride during the material synthesis to substitute and/or replace possible missing OH^- groups[14] in the inorganic cluster (Figure 1). We note that this result is similar to the previously demonstrated incorporation of chloride ions into the zirconium clusters of UiO-66, which led to the restoration of defects through substitution of some of the cornerstone hydroxide groups.[15a,b] The approach herein reported is in principle applicable to the entire UiO series of frameworks that have been synthesized previously. In addition, it has been suggested that fluoride acts as a mineralizing agent that favors the formation of highly crystalline phases in MOFs.[15c,d]

By performing the synthesis of **1** in the presence of NaF, we obtained a material with significantly increased thermal stability (see Figure S1), which may be attributed to F^- ions replacing the μ_3-OH^- units in the framework zirconium cluster. The later was confirmed by solid X-ray powder diffraction and N_2 adsorption isotherms. Also, increased thermal stability is observed during solvent exchanges and activation conditions. For instance, the lack of F^- ions during the synthesis of **1** led to diminished porosity and crystallinity of the framework above 50 °C during solvent exchanges, whereas the framework with F^- was heated at 80 °C for solvent exchange and does not shows sign of decomposition.

Elemental analysis suggested that as many as 49% of the OH^- units were replaced with F^-, while the crystallinity was observed to decrease significantly when higher loadings of NaF were attempted. Thus, it was not possible to replace 100% of the bridging OH^- with F^- ion. Additionally, the presence of chloride ions was detected by elemental analysis, even when the zwitterionic form of the ligand (NH_3−tpdc) was employed in the preparation of **1**. Given that the synthesis takes place in a strongly acidic solution, it is likely that methylamine functionalities on the ligand may react to form methylammonium salts with charge balancing chloride ions derived from the $ZrCl_4$ precursor. As we discuss further, the resulting ammonium salts may also inhibit **1** from exhibiting the expected CO_2 uptake.

Solid state NMR spectroscopy was employed to confirm the bulk composition of **1** (see Figure S2). The ^{13}C cross-polarization MAS NMR spectrum of **1** exhibits only six signals, in contrast to the eight signals expected for this material. We note that the aromatic signals from 140 to 120 ppm are very broad, which might be explained by orientation dependent interactions in the solid state due to the high density of methylamine groups present on the linkers. Hence, it was only possible to assign three peaks from the five expected in this region. Even still, the spectrum confirmed the presence of the organic linker in the structure of **1**. Additionally, the ^1H MAS NMR spectrum exhibits two broad peaks that were attributed to the aromatic and aliphatic protons.

Despite significant effort, we were unable to grow crystals of **1** suitable for single crystal diffraction. However, X-ray powder diffraction data confirm that the metal−organic framework crystallizes in the *Fm*-3m space group and is isostructural to UiO-68. The unit cell dimensions of **1** (a = 32.4668(3) Å, V = 34223(1) Å^3) were determined by performing a structureless Le Bail refinement as implemented in the EXPGUI/GSAS software package.[16] Note that this framework is also isostructural to PCN-57,[17] which contains four methyl substituents on the central ring of the terphenyl linker but has a 5% smaller unit cell volume.

While we were unable to fully solve the crystal structure of **1** from powder diffraction data, it was possible to gain insight into the arrangement of the methylamines inside the framework pores by calculating a Fourier difference map, using the experimental X-ray diffraction pattern of PCN-57 as a starting structural model. Excess electron density inside the pores near the central ring of the terphenyl linker is attributed to the amine functionalities of **1** (see Figure 2 and Figures S3−S5). Additional electron density observed between the amine groups is likely from Cl^-, wherein each Cl^- is capable of interacting with multiple $-NH_2$ or $-NH_3^+$ groups. Such an arrangement would be expected to make the amines inaccessible to guest molecules such as CO_2,[18] although the extra H^+ and Cl^-

DOI: 10.1021/acs.inorgchem.6b02745
Inorg. Chem. 2017, 56, 4308−4316

present in the pores might be displaced by washing with a strong base or by inserting metal cations to bind the $-NH_2$ functionalities.

In order to prevent the possible framework pore obstruction caused by the ammonium groups, we sought conditions to postsynthetically deprotonate the amines using a noncoordinating base. Although it has previously been observed that zirconium frameworks can exhibit a high stability toward water and strongly acidic or basic media,[10,12c,17,19] we found that **1** is quite sensitive to both humidity and changes in pH, most likely due to the basic and hydrophilic character of methylamine functionalities. For instance, while **1** is not soluble in an acidic solutions, crystallinity and porosity are indeed considerably diminished when **1** is exposed to acidic solutions. In addition, we have observed that material **1** exhibits significant affinity toward water (Figures S19–S21), leading to reduced crystallinity and gas-adsorptive properties.

Considering the aforementioned, careful selection of the base and reaction conditions was crucial to ensure that the deprotonation of the amines could be carried out without diminishing the crystallinity and porosity of the framework. As a result, we performed postsynthetic deprotonation using only the neutral organic bases 1,8-bis(dimethylamino)naphthalene (DMAN) or trimethylamine, which exhibit high pK_a values in organic solvents (pK_a = 18.62 and 18.82, respectively, in MeCN).[20]

Deprotonation of the zirconium metal–organic framework was carried out by soaking the framework in a 0.21 M acetonitrile solution of the base (DMAN or trimethylamine) at room temperature for 72 h. The solution was then immediately decanted, and the resulting solid was washed several times with fresh acetonitrile and THF. The solid was then heated at 135 °C under dynamic vacuum for 24 h to yield the activated framework **1**. To established activation conditions for compound **1** we screened temperatures from 60 to 145 °C, in a 5 °C steps under dynamic vacuum, finding that 135 °C is the best activation temperature for this material.

Analysis of the acetonitrile supernatant by ^{1}H NMR revealed the presence of protonated DMAN or triethylamine (Figure S7). Protonated DMAN was crystallized by solvent evaporation from the NMR tube (Figure S6). In support of the ^{1}H NMR data, single crystal X-ray diffraction measurements revealed the presence of chloride ions and protonated DMAN ($C_{14}H_{18}N_2H^+$). On the other hand, elemental analysis of the resulting material (**1**) treated with DMAN revealed the elimination of one Cl^- per formula unit.

Gas Adsorption. Activated **1** was prepared by first soaking the as-synthesized material in DMF at 80 °C, followed by THF at room temperature and finally heating at 135 °C under dynamic vacuum for 24 h. Low-pressure N_2 adsorption isotherm data collected at 77 K were used to calculate BET and Langmuir surface areas of 1908 m^2/g and 2215 m^2/g, respectively, thus confirming framework porosity. This surface area is significantly lower than that measured for UiO-68 (3741 m^2/g),[10] which is an expected result based on the high density of methylamine groups present in the pores of **1**. Gas adsorption isotherms collected at 25 °C (Figure 3) revealed that **1** has only a modest affinity for CO_2 at 0.15 bar (0.51 mmol/g; 2 wt %) and 1 bar (2.25 mmol/g; 9 wt %), which we attribute to the inaccessibility of the amine groups due to intramolecular hydrogen bonding and electrostatic interactions between chloride anions and protonated amine sites (Table 1, Figure S15).

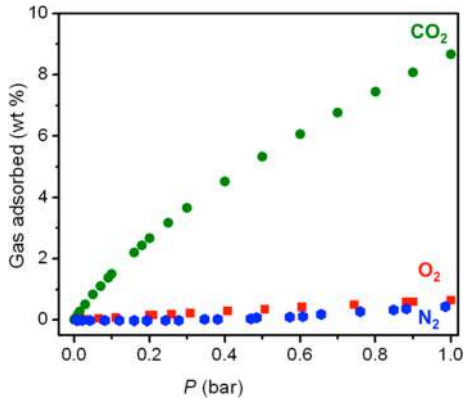

Figure 3. Adsorption isotherms for CO_2 (green circles), N_2 (blue circles), and O_2 (red squares) uptake in **1** at 25 °C.

The theoretical CO_2 uptake for **1** is 19 wt %, assuming accessibility of all the amines in the framework and a 1:1 reaction between CO_2 and the amine groups to form carbamic acid species. Further attempts to remove the remaining Cl^- using this deprotonation approach were unsuccessful, which could be due to difficulties in accessing all the protonated amines or due the possible chloride–ions interactions with multiple amine groups. On the other hand, we believe the proximity of the amine sites within the framework could instead facilitate the binding of CO_2 at two amine sites to form ammonium carbamates,[21,5f] which would correspond to 9.5 wt % as the highest theoretical CO_2 uptake. Note that, in our hands, efforts trying to determine the CO_2 adsorption mechanism by in situ IR were inconclusive, mainly because activated **1** readily adsorbs water, thereby impeding mechanistic studies for CO_2 (Figures S19 and S21).

The shapes of the CO_2 isotherms for **1** at low pressures do not reflect a strong interaction between the methylamine groups and CO_2, and thus we considered that hydrogen bonded amines and/or extra-framework anions might still be limiting the accessibility of CO_2 molecules to the primary amines within the framework pores.[22] Consistent with a lack of strong CO_2 adsorption sites, the isosteric heat of CO_2 adsorption (calculated using isotherm data collected at 298, 308, and 318 K) was found to be close to 35 kJ/mol **1**, which is well below that expected for the interaction of amine sites with CO_2 molecules.[5a,b]

Metal Binding. To further increase CO_2 uptake, we sought to use the methylamine moieties as chelating ligand sites for metal binding. Therefore, our first choice was to employ copper salts (e.g., $Cu(NCCH_3)_4{\cdot}CF_3SO_3$) to obtain the metalated frameworks. Note that metal incorporation of other Zr-MOFs has been reported elsewhere, although the approach employed for the preparation of these materials involves alkali metal binding.[23]

Compound **1** was soaked in an acetonitrile solution of $Cu(MeCN)_4{\cdot}CF_3SO_3$ to afford $Zr_6O_4(OH)_{2.1}F_{1.9}$(tpdc-$4CH_2NH_2{\cdot}1.9HCl)_6{\cdot}0.42Cu(MeCN)_4{\cdot}CF_3SO_3$ (**2**), as confirmed by elemental analysis and ICP-OES. Thermogravimetric analysis showed moderate thermal stability with a weight loss of 25% between room temperature and 110 °C, with no additional mass loss occurring until 165 °C. X-ray powder diffraction, solid-state NMR spectroscopy, and infrared spectroscopy additionally confirmed that the overall framework structure was unaffected by metal complexation (see Figures S10 and S11).

DOI: 10.1021/acs.inorgchem.6b02745
Inorg. Chem. 2017, 56, 4308–4316

Table 1. Main Characteristics of Material 1 under Different Activation Conditions

	Material **1**	
activation conditions	1. THF, 25 °C 2. 100 °C vacuo 12 h	1. DMAN, 72 h 2. THF, 25 °C 3. 100 °C vacuo 12 h
Langmuir surface area (m^2/g) at 77 K	1837	2215
BET surface area (m^2/g) at 77 K	1710	1908
CO_2 uptake (mmol/g; wt %) at 0.15 bar	0.40; 2.00	0.51; 2.25
CO_2 uptake (mmol/g; wt %) at 1.00 bar	1.75; 7.00	2.30; 9.00
pore volume (cm^3/g)	0.56	0.59

As expected, the metalated framework **2** exhibited reduced porosity, with a Langmuir surface area of 2054 m^2/g. In spite of its lower surface area **2** showed enhanced CO_2 uptake at 0.15 and 1 bar (0.9 mmol/g, 3.9 wt % and 2.9 mmol/g, 11.3 wt %, see Figure 4) compared to material **1**. Likewise, the selectivity

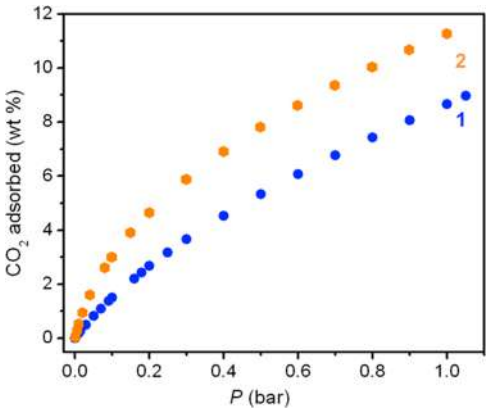

Figure 4. Adsorption isotherms collected at 25 °C for the uptake of CO_2 in **1** (blue circles) and **2** (yellow hexagons).

factor, S_{ads}, for adsorption of CO_2 over N_2 (calculated from the single-component isotherm data as the ratio of the adsorbed amount of CO_2 at 0.15 bar to the adsorbed amount of N_2 at 0.75 bar) increased from 21.2 in **1** to 54.1 in **2** (Figure S12). Note that the selectivity was normalized for the pressures chosen according to eq 1, where q_i is the uptake and p_i is the partial pressure of component *i*.

$$S_{ads} = \frac{q_1/q_2}{p_1/p_2} \quad (1)$$

We sought to further improve the CO_2 capacity of **2** by increasing Cu concentration from 7 mol % to 30 mol %; however, the resulting material exhibited a reduction in CO_2 uptake, adsorbing 0.67 mmol/g (2.9 wt %) at 0.15 bar and 2.34 mmol/g (9.3 wt %) at 1 bar (Figure S13). This decrease in CO_2 adsorption may be due to increased pore blockage upon incorporation of a greater amount of copper salt. Langmuir surface area is 1990 m^2/g.

Furthermore, we determine the zero-coverage isosteric heat of adsorption ($-Q_{st}$) for compound **1** and **2**. The $-Q_{st}$ is helpful for the CO_2 adsorption analysis since it provides an indication of the strength of the strongest binding sites within the material, which, depending on its magnitude can be attributed to certain chemical features of the pore surface, such as exposed metal cation sites or amine functionalities. In this case, isosteric heat of CO_2 adsorption for **2**, which present exposed cations, was found to be 29 kJ/mol at the lowest CO_2 loading. In comparison to other metal−organic frameworks its $-Q_{st}$ is higher than $-Q_{st}$ of CuBTTri (21 kJ/mol),[2b] but lower than Mg-MOF-74 (47 kJ/mol), Ni- MOF-74 (42 kJ/mol), and MIL-100 (Cr) (62 kJ/mol). On the other hand, the value of 33 kJ/mol determined for **1**, is lower than that reported for other metal−organic frameworks possessing amine functionalities. For instance, the postsynthetically modified, Cu-BTTri-mmen and Cu-BTTri-en, present a $-Q_{st}$ value of 96 and 90 kJ/mol, respectively.[2b] However, IRMOF-3 shows a value of 19 kJ/mol, meaning that CO_2 adsorptive process is not chemisorption.[2b] According to the values of **1** and **2** it is reasonable to classify their isosteric heat of adsorption as medium strength physisorption. Note as the CO_2 loading is increased, **2** also exhibit a roughly constant $-Q_{st}$ value, which is indicative of greater uniformity among the adsorption sites and in contrast to the gradual decline in $-Q_{st}$ observed for **1** (Figure 5). It is

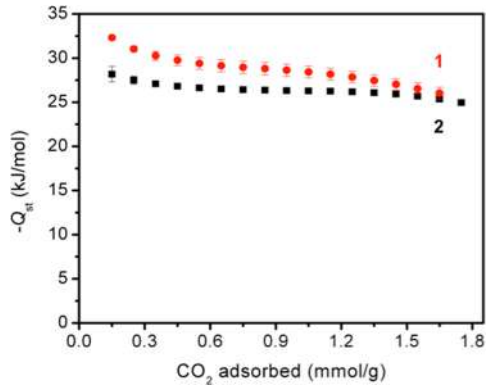

Figure 5. Isosteric heats of CO_2 adsorption ($-Q_{st}$) for **1** (red) and **2** (black) as a function of the amount of CO_2 adsorbed. Error bars are determined from fitting to the Clausius−Clapeyron equation.

possible that the copper insertion leads to a higher density of adsorption sites, on the pore surface, leading to greater CO_2 adsorption; however, such adsorption sites have slightly lower, average binding enthalpy, resulting in weaker interactions compared to the methylamine groups. Therefore, **2** exhibits higher CO_2 uptake but lower $-Q_{st}$, compared to **1**.

Subsequently, we tried other sources of copper. For instance, the reaction between **1** and $Cu(CF_3SO_3)_2$ yields the material $Zr_6O_4(OH)_{2.1}F_{1.9}(tpdc\text{-}4CH_2NH_2{\cdot}1.7HCl)_6{\cdot}1.8Cu(CF_3SO_3)_2$ (**3**), which exhibits 2.7 and 9.5 wt % CO_2 adsorption at 0.15 and 1 bar, respectively. Further attempts to load different concentrations of $Cu(CF_3SO_3)_2$ in **1** result in poorer CO_2 uptakes.

DOI: 10.1021/acs.inorgchem.6b02745
Inorg. Chem. 2017, 56, 4308−4316

CONCLUSIONS

We successfully synthesized the porous zirconium framework **1**, which possesses a high density of primary amine functionalities covalently attached to the bridging organic linkers. In spite of the high alkylamine content of the organic linker used in the synthesis of the framework, the resulting material shows only modest CO_2 uptake at low pressures. This low uptake could be a result of the formation of ammonium salts within the pores, which prevent higher CO_2 uptake or closely spaced methylamine groups that exhibit strong intra- and interatomic hydrogen bonding, similarly preventing a strong interaction with CO_2. However, complexation of 7 mol % of $Cu(MeCN)_4 \cdot CF_3SO_3$ in **1** yields an increase in CO_2 adsorption mostly due the interaction between copper and CO_2 despite the reduced porosity associated with incorporation of the copper salt.

The results herein demonstrate the intrinsic complications in designing metal−organic frameworks with a high density of amines and the importance of proper activation. Indeed, contrary to our initial hypothesis, a high density of amine functionalities within the pores of a framework does not necessarily afford superior CO_2 uptake. When novel materials for CO_2 capture are designed, it is essential to consider not only the chemical functionalities that will selectively interact with CO_2 but also any secondary interactions that may prevent a material from exhibiting the optimal gas uptake. For instance, primary amines might have stronger hydrogen bonding interactions than secondary amines, thus impeding a strong interaction with CO_2. These findings may also apply to mesoporous materials, grafted with a high density of primary and secondary amines, which normally exhibit lower CO_2 adsorption capacities than expected.[5g,18,24]

The evaluation of amine-appended frameworks exhibiting a lower density of primary-amine functionalities on the pore surface may lead to more stable materials as well as new insights in understanding the mechanisms for CO_2 adsorption in amine-functionalized porous materials. On the other hand, the study of the behavior of materials with appended secondary amines might be of interest to establish a correlation between the strength of the hydrogen bonding interactions and the accessibility of the free electron pairs on the amine substituents. Finally, it would be interesting to test the incorporation of other metal cations onto material **1**, which may lead to a broad range of applications other than CO_2 capture, such as catalysis and gas adsorption.

ASSOCIATED CONTENT

Supporting Information

The Supporting Information is available free of charge on the ACS Publications website at DOI: 10.1021/acs.inorgchem.6b02745.

Powder and single crystal X-ray diffraction data, additional CO_2 and N_2 isotherms and fits, isosteric heat of adsorption calculations, FTIR spectra, TGA measurements, and NMR characterization (PDF)

AUTHOR INFORMATION

Corresponding Author

*E-mail: p.gomora@unam.mx.

ORCID

A. Paulina Gómora-Figueroa: 0000-0003-1487-8204

Notes

The authors declare no competing financial interest.

ACKNOWLEDGMENTS

Use of the Advanced Photon Source (APS), an Office of Science User Facility operated for the U.S. DoE Office of Science by Argonne National Laboratory, was supported by the U.S. DoE under Contract DE-AC02-06CH11357. We thank Dr. Wendy Queen, Dr. Matt Hudson, and Dr. Greg Halder for assisting with the collection of diffraction data on 1-BM-C at the APS. "This research was supported by the Center for Gas Separations Relevant to Clean Energy Technologies, an Energy Frontier Research Center funded by the U.S. Department of Energy, Office of Science, Office of Basic Energy Sciences, under Award DE-SC0001015." A.P.G. acknowledges Schlumberger FFTF Fellowship. We thank NSF for providing graduate fellowship support for J.A.M. Single-crystal X-ray diffraction measurements were conducted at the Advanced Light Source facility at the Lawrence Berkeley National Laboratory, which is supported by the Director, Office of Science, Office of Basic Energy Sciences, of the U.S. Department of Energy under Contract No. DE-AC02-05CH11231. We give special acknowledgement to Prof. Jeffrey R. Long for support and advice.

REFERENCES

(1) (a) Climate Change 2007: The Physical Science. In *The Fourth Assessment Report of the Intergovernmental Panel on Climate Change*; Basis; Solomon, S., Qin, D., Manning, M., Chen, Z., Marquis, M., Averyt, K. B., Tignor, M., Miller, H. L., Eds.; Cambridge University Press: New York, 2007. (b) International Energy Agency's Directorate of Sustainable Energy Policy and Technology. *Energy Technology Perspectives 2012: Pathways to a Clean Energy System*; Paris, France, 2012.

(2) (a) Haszeldine, R. S. Carbon Capture and Storage: How Green Can Black Be? *Science* **2009**, *325*, 1647−1652. (b) Sumida, K.; Rogow, L. D.; Mason, J. A.; McDonald, T. M.; Bloch, E. D.; Herm, Z. R.; Bae, T.-H.; Long, R. J. Carbon Dioxide Capture in Metal−Organic Frameworks. *Chem. Rev.* **2012**, *112*, 724−781.

(3) (a) Dupart, M. S.; Bacon, T. R.; Edwards, D. J. Understanding Corrosion in Alkanolamine Gas Treating Plants, Parts 1 and 2. *Hydrocarbon Processing* **1993**, May, 75−80. (b) Rochelle, G. T. Amine Scrubbing for CO_2 Capture. *Science* **2009**, *325*, 1652−1654. (c) Ciferno, J.; Litynski, J.; Plasynski, S.; Murphy, J.; Vaux, G.; Munson, R.; Marano, R. *Carbon Dioxide Capture and Storage RD&D Roadmap*; U.S. DOE National Energy Technology Laboratory: Pittsburgh, PA, December, 2010. (d) Krutka, H.; Sjostrom, S. ADA Environmental Solutions, *Evaluation of Solid Sorbents as Retrofit Technology for CO_2 Capture from Coal-Fired Power Plants*, October 2011, 10.2172/1084028

(4) (a) Figueroa, J. D.; Fout, T.; Plasynski, S.; McIlvried, H.; Srivastava, R. D. Advances in CO_2 capture technology—The U.S. Department of Energy's Carbon Sequestration Program. *Int. J. Greenhouse Gas Control* **2008**, *2*, 9−20. (b) D'Alessandro, D. M.; Smit, B.; Long, J. R. Carbon dioxide capture: prospects for new materials. *Angew. Chem., Int. Ed.* **2010**, *49*, 6058−6082.

(5) (a) Hicks, J. C.; Drese, J. H.; Fauth, D. J.; McMahan, L. G.; Qi, G.; Jones, C. W. Designing adsorbents for CO_2 capture from flue gas-hyperbranched aminosilicas capable of capturing CO_2 reversibly. *J. Am. Chem. Soc.* **2008**, *130*, 2902−2903. (b) Yue, M. B.; Sun, L. B.; Wang, Z. J.; Wang, Y.; Yu, Q.; Zhu, J. H. Promoting the CO_2 adsorption in the amine-containing SBA-15 by hydroxyl group. *Microporous Mesoporous Mater.* **2008**, *114*, 74−81. (c) Demessence, A.; D'Alessandro, D. M.; Foo, M. L.; Long, J. R. Strong CO_2 Binding in a Water-Stable, Triazolate-Bridged Metal−Organic Framework Functionalized with Ethylenediamine. *J. Am. Chem. Soc.* **2009**, *131*, 8784−8786. (d) Sayari, A.; Belmabkhout, Y. Stabilization of Amine-

DOI: 10.1021/acs.inorgchem.6b02745
Inorg. Chem. 2017, 56, 4308−4316

Containing CO_2 Adsorbents: Dramatic Effect of Water Vapor. *J. Am. Chem. Soc.* **2010**, *132*, 6312−6314. (e) Bhagiyalakshmi, M.; Anuradha, R.; Park, S. D.; Jang, H. T. Octa(aminophenyl)silsesquioxane fabrication on chlorofunctionalized mesoporous SBA-15 for CO_2 adsorption. *Microporous Mesoporous Mater.* **2010**, *131*, 265−273. (f) McDonald, T. M.; D'Alessandro, M. D.; Krishna, R.; Long, J. R. Enhanced carbon dioxide capture upon incorporation of *N,N′*-dimethylethylenediaminein the metal−organic framework CuBTTri. *Chem. Sci.* **2011**, *2*, 2022−2028. (g) Danon, A.; Stair, P. C.; Weitz, E. FTIR Study of CO_2 Adsorption on Amine-Grafted SBA-15: Elucidation of Adsorbed Species. *J. Phys. Chem. C* **2011**, *115*, 11540−11549. (h) McDonald, T. M.; Lee, W. R.; Mason, J. A.; Wiers, B. M.; Hong, C. S.; Long, J. R. Capture of Carbon Dioxide from Air and Flue Gas in the Alkylamine-Appended Metal−Organic Framework mmen-Mg_2(dobpdc). *J. Am. Chem. Soc.* **2012**, *134*, 7056−7065.

(6) (a) Dietzel, P. D. C; Johnsen, R. E.; Blom, R.; Fjellvåg, H. Structural Changes and Coordinatively Unsaturated Metal Atoms on Dehydration of Honeycomb Analogous Microporous Metal−Organic Frameworks. *Chem. - Eur. J.* **2008**, *14*, 2389−2397. (b) Vitillo, J. G.; Regli, L.; Chavan, S.; Richiardi, G.; Spoto, G.; Dietzel, P.D. C.; Bordiga, S.; Zecchina, A. Role of Exposed Metal Sites in Hydrogen Storage in MOFs. *J. Am. Chem. Soc.* **2008**, *130*, 8386−8396. (c) Zhou, W.; Wu, H.; Yildirim, T. Enhanced H_2 Adsorption in Isostructural Metal−Organic Frameworks with Open Metal Sites: Strong Dependence of the Binding Strength on Metal Ions. *J. Am. Chem. Soc.* **2008**, *130*, 15268−15269. (d) Bae, Y.-S.; Lee, C. Y.; Kim, K. C.; Farha, O. K.; Nicklas, P.; Hupp, J. T.; Nguyen, S.; Snurr, R. Q. High Propene/Propane Selectivity in Isostructural Metal-Organic Frameworks with High Densities of Open Metal Sites. *Angew. Chem., Int. Ed.* **2012**, *51*, 1857−1860. (e) Li, Y.-W.; Li, J.-R.; Wang, L.-F.; Zhou, B.-Y.; Chen, Q.; Bu, Z.-H. Microporous metal−organic frameworks with open metal sites as sorbents for selective gas adsorption and fluorescence sensors for metal ions. *J. Mater. Chem. A* **2013**, *1*, 495−499. (f) Duan, X.; Cai, J.; Yu, J.; Wu, C.; Cui, Y.; Qian, G. Three-dimensional copper (II) metal−organic framework with open metal sites and anthracene nucleus for highly selective C_2H_2/CH_4 and C_2H_2/CO_2 gas separation at room temperature. *Microporous Mesoporous Mater.* **2013**, *181*, 99−104. (g) Queen, W. L.; Bloch, E. D.; Brown, C. M.; Hudson, M. R.; Mason, J. A.; Murray, L. J.; Ramirez-Cuesta, A. J.; Peterson, V. K.; Long, J. R. Hydrogen adsorption in the metal−organic frameworks Fe_2(dobdc) and $Fe_2(O_2)$ (dobdc). *Dalton Trans.* **2012**, *41*, 4180−4187. (h) Cai, J.; Yu, J.; Xu, H.; He, Y.; Duan, X.; Cui, Y.; Wu, C.; Chen, B.; Qian, G. A Doubly Interpenetrated Metal−Organic Framework with Open Metal Sites and Suitable Pore Sizes for Highly Selective Separation of Small Hydrocarbons at Room Temperature. *Cryst. Growth Des.* **2013**, *13*, 2094−2097. (i) Kapelewski, M. T.; Geier, S. J.; Hudson, M. R.; Stück, D.; Mason, J. A.; Nelson, J. N.; Xiao, D. J.; Hulvey, Z.; Gilmour, E.; FitzGerald, S. A.; Head-Gordon, M.; Brown, C. M.; Long, J. R. M_2(*m*-dobdc) (M = Mg, Mn, Fe, Co, Ni) Metal−Organic Frameworks Exhibiting Increased Charge Density and Enhanced H_2 Binding at the Open Metal Sites. *J. Am. Chem. Soc.* **2014**, *136*, 12119−12129. (j) Bloch, E. D.; Hudson, M. R.; Mason, J. A.; Chavan, S.; Crocellà, V.; Howe, J. D.; Lee, K.; Dzubak, A. L.; Queen, W. L.; Zadrozny, J. M.; Geier, S. J.; Lin, L.-C.; Gagliardi, L.; Smit, B.; Neaton, J. B.; Bordiga, S.; Brown, C. M.; Long, J. R. Reversible CO binding enables tunable CO/H_2 and CO/N_2 separations in metal−organic frameworks with exposed divalent metal cations. *J. Am. Chem. Soc.* **2014**, *136*, 10752−10761.

(7) (a) Dincă, M.; Dailly, A.; Liu, Y.; Brown, C. M.; Neumann, D. A.; Long, J. R. Hydrogen Storage in a Microporous Metal-Organic Framework with Exposed Mn^{2+} Coordination Sites. *J. Am. Chem. Soc.* **2006**, *128*, 16876−16883. (b) Szeto, K. C.; Kongshaug, K. O.; Jakobsen, S.; Tilset, M.; Lillerud, K. P. Design, Synthesis and Characterization of a Pt−Gd Metal−Organic Framework Containing Potentially Catalytically Active Sites. *Dalton Trans.* **2008**, *15*, 2054−2060. (c) Caskey, S. R.; Wong-Foy, A. G.; Matzger, A. J. Dramatic Tuning of Carbon Dioxide Uptake via Metal Substitution in a Coordination Polymer with Cylindrical Pores. *J. Am. Chem. Soc.* **2008**, *130*, 10870−10871. (d) Doonan, C. J.; Morris, W.; Furukawa, H.; Yaghi, O. M. Isoreticular Metalation of Metal−Organic Frameworks. *J. Am. Chem. Soc.* **2009**, *131*, 9492−9493. (e) Debatin, F.; Thomas, A.; Kelling, A.; Hedin, N.; Bacsik, Z.; Senkovska, I.; Kaskel, S.; Junginger, M.; Müller, H.; Schilde, U.; Jäger, C.; Friedrich, A.; Holdt, H. J. In Situ Synthesis of an Imidazolate-4-amide-5-imidate Ligand and Formation of a Microporous Zinc−Organic Framework with H_2-and CO_2-Storage Ability. *Angew. Chem., Int. Ed.* **2010**, *49*, 1258−1262. (f) Murray, L. J.; Dincă, M.; Yano, J.; Chavan, S.; Bordiga, S.; Brown, C. M.; Long, J. R. Highly-Selective and Reversible O_2 Binding in Cr_3(1,3,5-benzenetricarboxylate)$_2$. *J. Am. Chem. Soc.* **2010**, *132*, 7856−7857.

(8) McDonald, T. M.; Mason, J. A.; Kong, X.; Bloch, E. D.; Gygi, D.; Dani, A.; Crocellà, V.; Giordano, F.; Odoh, S.; Drisdell, W.; Vlaisavljevich, B.; Dzubak, A. L.; Poloni, R.; Schnell, S. K.; Planas, N.; Lee, K.; Pascal, T.; Wan, L. F.; Prendergast, D.; Neaton, J. B.; Smit, B.; Kortright, J. B.; Gagliardi, L.; Bordiga, S.; Reimer, J. A.; Long, J. R. Cooperative insertion of CO_2 in diamine-appended metal-organic frameworks. *Nature* **2015**, *519*, 303−308.

(9) Bloch, E. D.; Britt, D.; Lee, C.; Doonan, C. J.; Uribe-Romo, F. J.; Furukawa, H.; Long, J. R.; Yaghi, O. M. Metal Insertion in a Microporous Metal−Organic Framework Lined with 2,2′-Bipyridine. *J. Am. Chem. Soc.* **2010**, *132*, 14382−14384.

(10) (a) Cavka, J. H.; Jakobsen, S.; Olsbye, U.; Guillou, N.; Lamberti, C.; Bordiga, S.; Lillerdu, P. A New Zirconium Inorganic Building Brick Forming Metal Organic Frameworks with Exceptional Stability. *J. Am. Chem. Soc.* **2008**, *130*, 13850−13851. (b) Schaate, A.; Roy, P.; Godt, A.; Lippke, J.; Waltz, F.; Wiebcke, M.; Behrens, P. Modulated Synthesis of Zr-Based Metal−Organic Frameworks: From Nano to Single Crystals. *Chem. - Eur. J.* **2011**, *17*, 6643−6651.

(11) (a) Fracaroli, M. A.; Furukawa, H.; Suzuki, M.; Dodd, M.; Okajima, S.; Gándara, F.; Reimer, J. A.; Yaghi, O. M. Metal−Organic Frameworks with Precisely Designed Interior for Carbon Dioxide Capture in the Presence of Water. *J. Am. Chem. Soc.* **2014**, *136*, 8863−8866. (b) Lin, Y.; Kong, C.; Chen, L. Amine-functionalized metal−organic frameworks: structure, synthesis and applications. *RSC Adv.* **2016**, *6*, 32598−32614.

(12) (a) Wu, H.; Chua, Y. S.; Krungleviciute, V.; Tyagi, M.; Chen, P.; Yildirim, T.; Zhou, W. Unusual and Highly Tunable Missing-Linker Defects in Zirconium Metal−Organic Framework UiO-66 and Their Important Effects on Gas Adsorption. *J. Am. Chem. Soc.* **2013**, *135*, 10525−10532. (b) Bai, Y.; Dou, Y.; Xie, L.-H.; Rutledge, W.; Li, J.-R.; Zhou, H.-C. Zr-based metal-organic frameworks: design, synthesis, structure and applications. *Chem. Soc. Rev.* **2016**, *45*, 2327−2367. (c) DeCoste, J. B.; Peterson, G. W.; Jasuja, H.; Golver, T. G.; Huang, Y.; Walton, K. S. Stability and degradation mechanisms of metal-organic frameworks containing the $Zr_6O_4(OH)_4$ secondary building unit. *J. Mater. Chem. A* **2013**, *1*, 5642−5650. (d) Øien, S.; Wragg, D.; Reinsh, H.; Svelle, S.; Bordiga, S.; Lamberti, C.; Lilleurd, K. P. Detailed Structure Analysis of Atomic Positions and Defects in Zirconium Metal-Organic Frameworks. *Cryst. Growth Des.* **2014**, *14*, 5370−5372.

(13) For instance, it was observed that HNO_3 lead to the formation of a stable and very crystalline material, though with diminished porosity. Further activation was unsuccessful and pores remained blocked, presumably due to strong ionic interactions inside the pores. The use of other acid sources yielded materials with poor crystallinity.

(14) Note the hydrogen atoms of the bridging groups have not been located, although analysis of Zr−O bond distances and the charge balance indicates the presence of four μ^3-OH groups. See, for example, (a) Kickelbick, G.; Schubert, U. Hydroxy carboxylate substituted oxozirconium clusters. *J. Chem. Soc., Dalton Trans.* **1999**, 1301−1306. (b) Piszczek, P.; Radtke, A.; Grodzicki, A.; Wojtczack, A.; Chojnacki, J. The New Type Of $[Zr_6(M_3\text{-}O)_4(M_3\text{-}OH)_4]$ Cluster Core: Crystal Structure And Spectral Characterization Of $[Zr_6O_4(OH)_4(OOCR)_{12}]$ (R = Bu^t, $C(CH_3)_2Et$). *Polyhedron* **2007**, *26*, 679−685.

(15) (a) Shearer, G. C.; Forselv, S.; Chavan, S.; Bordiga, S.; Mathisen, K.; Bjørgen, M.; Svelle, S.; Lillerud, K. P. In Situ Infrared Spectroscopic and Gravimetric Characterisation of the Solvent Removal and Dehydroxylation of the Metal Organic Frameworks UiO-66 and UiO-67. *Top. Catal.* **2013**, *56*, 770−782. (b) Vermoortele,

DOI: 10.1021/acs.inorgchem.6b02745
Inorg. Chem. 2017, 56, 4308−4316

F.; Bueken, B.; Le Bars, G.; Van de Voorde, B.; Vandichel, M.; Houthoofd, K.; Vimont, A.; Daturi, M.; Waroquier, M.; Van Speybroeck, V.; Kirschhock, C.; De Vos, D. E. Synthesis Modulation as a Tool To Increase the Catalytic Activity of Metal−Organic Frameworks: The Unique Case of UiO-66(Zr). *J. Am. Chem. Soc.* **2013**, *135*, 11465−11468. (c) Loiseau, T.; Férey, G. Crystalline oxyfluorinated open-framework compounds: Silicates, metal phosphates, metal fluorides and metal-organic frameworks (MOF). *J. Fluorine Chem.* **2007**, *128*, 413−422. (d) Hong, D. Y.; Hwang, Y. K.; Serre, C.; Férey, G.; Chang, J. S. Porous Chromium Terephthalate MIL-101 with Coordinatively Unsaturated Sites: Surface Functionalization, Encapsulation, Sorption and Catalysis. *Adv. Funct. Mater.* **2009**, *19*, 1537−1552. (e) Juan-Alcañiz, J.; Gielisse, R.; Lago, A. B.; Ramos-Fernandez, E. V.; Serra-Crespo, P.; Devic, T.; Guillou, N.; Serre, C.; Kapteijn, F.; Gascon, J. Towards acid MOFs − catalytic performance of sulfonic acid functionalized architectures. *Catal. Sci. Technol.* **2013**, *3*, 2311−2318.

(16) (a) Larson, A. C.; Von Dreele, R. B. *General Structure Analysis System (GSAS)*, Report LAUR, 86-784, Los Alamos National Laboratory, 2004. (b) Toby, B. H. *EXPGUI*, a graphical user interface for *GSAS*. *J. Appl. Crystallogr.* **2001**, *34*, 210−213.

(17) Jiang, H.-L.; Feng, D.; Liu, T.-F.; Li, J.-R.; Zhou, H.-C. Pore Surface Engineering with Controlled Loadings of Functional Groups via Click Chemistry in Highly Stable Metal−Organic Frameworks. *J. Am. Chem. Soc.* **2012**, *134*, 14690−14693.

(18) (a) Chatt, J.; Duncanson, L. A.; Venanzi, L. M. An infrared spectroscopic investigation of absorption due to the N−H stretching modes of vibration in co-ordination compounds of ammonia and amines. Hydrogen bonding (N−H···Cl) in a series of amine complexes of platinous chloride. *J. Chem. Soc.* **1956**, *0*, 2712−2725. (b) Dubois, L. H.; Nuzzo, R. G. Synthesis, Structure, and Properties of Model Organic Surfaces. *Annu. Rev. Phys. Chem.* **1992**, *43*, 437−463. (c) Jockusch, R. A.; Lemoff, A. S.; Williams, E. R. Effect of Metal Ion and Water Coordination on the Structure of a Gas-Phase Amino Acid. *J. Am. Chem. Soc.* **2001**, *123*, 12255−12265. (d) Kamariotis, A.; Boyarkin, O. V.; Mercier, S. R.; Beck, R. D.; Bush, M. F.; Williams, E. R.; Rizzo, T. R. Infrared Spectroscopy of Hydrated Amino Acids in the Gas Phase: Protonated and Lithiated Valine. *J. Am. Chem. Soc.* **2006**, *128*, 905−916. (e) Rocher, N.; Frech, R. Hydrogen Bonding and Cation Coordination Effects in Primary and Secondary Amines Dissolved in Carbon Tetrachloride. *J. Phys. Chem. A* **2007**, *111*, 2662−2669.

(19) (a) Huang, Y.; Qin, W.; Li, Z.; Li, Y. Enhanced stability and CO_2 affinity of a UiO-66 type metal−organic framework decorated with dimethyl groups. *Dalton Trans.* **2012**, *41*, 9283−9285. (b) Wu, H.; Yildirim, T.; Zhou, W. Exceptional Mechanical Stability of Highly Porous Zirconium Metal−Organic Framework UiO-66 and Its Important Implications. *J. Phys. Chem. Lett.* **2013**, *4*, 925−930.

(20) According to the literature, DMAN leads to a gradual increase in basicity on account of strain effects, allowing intramolecular hydrogen bonding and relieving the steric strain upon protonation by geometrical effects. (a) Alder, R. W.; Bowman, P. S.; Steele, R. S.; Winterman, D. R. The Remarkable Basicity Of 1, 8-Bis (Dimethylamino) Naphthalene. *Chem. Commun.* **1968**, *13*, 723−724. (b) Alder, R. W. Strain Effects On Amine Basicities. *Chem. Rev.* **1989**, *89*, 1215−1223. (c) Mallinson, P. R.; Woźniak, K.; Smith, G. T.; McCormack, K. L. A charge density analysis of cationic and anionic hydrogen bonds in a "proton sponge" comple. *J. Am. Chem. Soc.* **1997**, *119*, 11502−11509. (d) Kaljurand, I.; Kütt, A.; Sooväli, L.; Rodima, T.; Mäemets, V.; Leito, I.; Koppel, I. A. Extension Of The Self-Consistent Spectrophotometric Basicity Scale In Acetonitrile To A Full Span Of 28 P K A Units: Unification Of Different Basicity Scales. *J. Org. Chem.* **2005**, *70*, 1019−1028.

(21) Sayari, A.; Heydari-Gorji, A.; Yang, Y. CO_2-Induced Degradation of Amine-Containing Adsorbents: Reaction Products and Pathways. *J. Am. Chem. Soc.* **2012**, *134*, 13834−13842.

(22) Brunelli, N. A.; Didas, S. A.; Venkatasubbaiah, K.; Jones, C. W. Tuning Cooperativity by Controlling the Linker Length of Silica-Supported Amines in Catalysis and CO_2 Capture. *J. Am. Chem. Soc.* **2012**, *134*, 13950−13953.

(23) (a) Hu, Z.; Zhang, K.; Zhang, M.; Guo, Z.; Jiang, J.; Zhao, D. A Combinatorial Approach towards Water-Stable Metal−Organic Frameworks for Highly Efficient Carbon Dioxide Separation. *ChemSusChem* **2014**, *7*, 2791−2795. (b) Hu, Z.; Faucher, S.; Zhou, Y.; Sun, Y.; Wang, S.; Zhao, D. Combination of Optimization and Metalated-Ligand Exchange: An Effective Approach to Functionalize UiO-66 (Zr) MOFs for CO_2 Separation. *Chem. - Eur. J.* **2015**, *21*, 17246−17255.

(24) The exposure mesoporous materials containing amines to CO_2 under dry conditions results in the deactivation of the amine groups via the formation of urea linkages. Materials containing primary amines are most likely to deactivate through an isocyanate intermediate followed by reaction with primary or secondary amines into di- and trisubstituted open-chain ureas. However, it is conceivable that deactivation of the materials may be avoided via the use of humidified gases. For more information see (a) Serna-Guerrero, R.; Da'na, E.; Sayari, A. New Insights into the Interactions of CO_2 with Amine-Functionalized Silica. *Ind. Eng. Chem. Res.* **2008**, *47*, 9406−9412. (b) Ko, Y. G.; Shin, S. S.; Choi, U. S. Primary, Secondary, And Tertiary Amines For CO_2 Capture: Designing For Mesoporous CO_2 Adsorbents. *J. Colloid Interface Sci.* **2011**, *361*, 594−599. (c) Sayari, A.; Belmabkhout, Y.; Da'na, E. CO_2 Deactivation of Supported Amines: Does the Nature of Amine Matter? *Langmuir* **2012**, *28*, 4241−4247.

DOI: 10.1021/acs.inorgchem.6b02745
Inorg. Chem. 2017, 56, 4308−4316